Applied Surface Science 470 (2019) 129–134

Contents lists available at ScienceDirect

Applied Surface Science

journal homepage: www.elsevier.com/locate/apsusc

Full Length Article

# Low-temperature wafer-scale growth of $MoS_2$-graphene heterostructures

Hyeong-U Kim[a], Mansu Kim[b], Yinhua Jin[a], Yuhwan Hyeon[a], Ki Seok Kim[b], Byeong-Seon An[b], Cheol-Woong Yang[b], Vinit Kanade[a], Ji-Yun Moon[c], Geun Yong Yeom[a,b], Dongmok Whang[a,b], Jae-Hyun Lee[c,*], Taesung Kim[a,d,*]

[a] SKKU Advanced Institute of Nanotechnology (SAINT), Sungkyunkwan University, Suwon 16419, South Korea
[b] School of Advanced Materials Science and Engineering, Sungkyunkwan University, Suwon 16419, South Korea
[c] Department of Energy Systems Research and Department of Materials Science and Engineering, Ajou University, Suwon 16499, South Korea
[d] School of Mechanical Engineering, Sungkyunkwan University, Suwon 16419, South Korea

ARTICLE INFO

*Keywords:*
$MoS_2$
Graphene
Heterostructure
Large-scale
PECVD
Hydrogen evolution reaction

ABSTRACT

In this study, we successfully demonstrate the fabrication of a $MoS_2$-graphene heterostructure (MGH) on a 4 inch wafer at 300 °C by depositing a thin Mo film seed layer on graphene followed by sulfurization using $H_2S$ plasma. By utilizing Raman spectroscopy and high-resolution transmission electron microscopy, we have confirmed that 5–6 $MoS_2$ layers with a large density of sulfur vacancies are grown uniformly on the entire substrate. The chemical composition of $MoS_2$ on graphene was evaluated by X-ray photoelectron spectroscopy, which confirmed the atomic ratio of Mo to S to be 1:1.78, which is much lower than the stoichiometric value of 2 from standard $MoS_2$. To exploit the properties of the nanocrystalline and defective MGH film obtained in our process, we have utilized it as a catalyst for hydrodesulfurization and as an electrocatalyst for the hydrogen evolution reaction. Compared to $MoS_2$ grown on an amorphous $SiO_2$ substrate, the MGH has smaller onset potential and Tafel slope, indicating its enhanced catalytic performance. Our practical growth approach can be applied to other two-dimensional crystals, which are potentially used in a wide range of applications such as electronic devices and catalysis.

## 1. Introduction

Realization of two-dimensional (2D) heterostructures has been intensively studied in view of their unique chemical, physical, and electrical properties [1–4]. Thus far, the main strategy for the preparation of a 2D heterostructure has been based on the sequential stacking of the layered materials using wet or dry transfer methods [5,6]. Ideally, this method allows for a conceptually new class of flexible and transparent films, with applications in batteries, electronic devices, and electrochemical cells [7–9]. However, these methods require time-consuming and complicated transfer processes, which also generate defects or residues at the interface of the 2D heterostructure [10]. The conventional thermal chemical vapor deposition (CVD) method using thermal decomposition of feedstocks, is considered a practical approach for the manufacture of 2D materials, whereby high-quality atomic scale heterostructures over large area can be obtained [11]. In particular, graphene, which is flexible, transparent, and highly conductive, is an ideal template to synthesize various transition metal dichalcogenide (TMDC) materials [12–14]. However, CVD reactions need relatively high growth temperatures (600–1000 °C) [15–17], which is incompatible with the complementary metal-oxidesemiconductor (CMOS) process and can therefore increase the total thermal budget in device fabrication [18–20]. To overcome this limitation, plasma-enhanced CVD (PECVD)-based synthesis technique has been introduced for 2D materials [21,22]. Although initial installation cost of PECVD system is higher than that of typical CVD system, in the presence of accelerated energetic electrons, excited molecules, free radicals, photons, and other active species in the plasma, the controlled growth of 2D materials can be realized at a relatively lower temperature. Our group recently demonstrated the low-temperature growth of uniform $MoS_2$ on a flexible plastic substrate [23,24].

In view of its tunable band gap and relatively high carrier mobility, $MoS_2$ has been investigated for applications in future electronic devices [25]. In addition, defects and edges of $MoS_2$ on the basal plane can act as active catalyst for hydro-desulfurization, due to which $MoS_2$ is considered as a strong candidate to replace currently used noble Pt catalyst [4,26]. Since Pt, which is considered as the best catalyst for HER, is low in natural abundance and high in cost, alternative catalysts

* Corresponding authors at: SKKU Advanced Institute of Nanotechnology (SAINT), Sungkyunkwan University, Suwon 16419, South Korea (T. Kim).
*E-mail addresses:* jaehyunlee@ajou.ac.kr (J.-H. Lee), tkim@skku.edu (T. Kim).

https://doi.org/10.1016/j.apsusc.2018.11.126
Received 5 July 2018; Received in revised form 12 November 2018; Accepted 15 November 2018
Available online 15 November 2018
0169-4332/ © 2018 Published by Elsevier B.V.

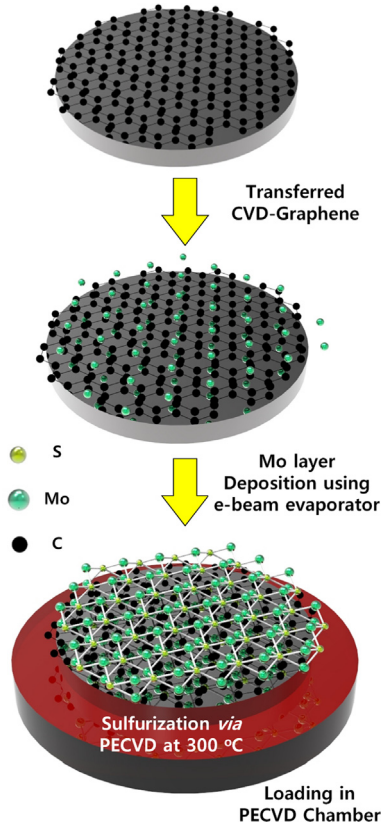


**Fig. 1.** Schematic illustration of the synthesis of the uniform MGH film via PECVD at 300 °C.

such as metal alloys, TMDs, and composite with TMDs were developed [9,27]. In particular, the combination of $MoS_2$ with graphene opens up new possibilities in electronic applications and also shows great potential as a catalyst [12,13,28–32]. To the best of our knowledge, however, the direct wafer-scale growth of $MoS_2$ on graphene at temperatures compatible with CMOS technology has not yet been reported. In this study, we demonstrate the fabrication of a $MoS_2$-graphene heterostructure (MGH) on a 4 inch wafer at 300 °C. A thin Mo film, which functions as a seed layer, was deposited on transferred graphene using e-beam evaporation after which, sulfurization was carried out using $H_2S$ plasma. Raman spectroscopy and high-resolution transmission electron microscopy (HR-TEM) were used to confirm that $MoS_2$ layers are uniformly grown on the entire substrate. The chemical composition of $MoS_2$ on graphene was determined by X-ray photoelectron spectroscopy (XPS); observed XPS data confirmed that the atomic ratio of Mo to S was 1:1.78, which is far beyond the stoichiometric value of the standard $MoS_2$. To exploit the unique properties of the nanocrystalline MGH film with high density of sulfur vacancy, we tested it as a catalyst for hydrodesulfurization and as an electro-catalyst for the hydrogen evolution reaction (HER) [33].

## 2. Experimental

### 2.1. Growth and transfer of monolayer graphene.

Graphene was synthesized on Cu foils (25 μm-thick, Alpha Aesar, 99.99% purity) using a conventional CVD process. Cu foils were placed in a 4 inch diameter quartz tube and after evacuation, $H_2$ (8 sccm, 99.999%) was introduced into the chamber and the Cu foil was annealed at 1040 °C for 2 h to remove residual impurities. Next, graphene growth was carried out on the Cu foil for 1 h by injecting 30 sccm of $CH_4$ and 50 sccm of $H_2$. Finally, the furnace was rapidly cooled to room temperature under $H_2$ atmosphere. To transfer the CVD-grown graphene layer from the Cu foil, the as-grown graphene sample was coated with a support layer of poly(methyl methacrylate) (PMMA, Microchem) by spin coating. The Cu foil was dissolved in aqueous iron (III) chloride ($FeCl_3$) solution and the PMMA-coated graphene was washed several times with deionized (DI) water before transferring it onto a $SiO_2$/Si wafer. The PMMA film was then completely dissolved in acetone.

### 2.2. Direct growth of $MoS_2$-graphene heterostructure (MGH)

Growth of the MGH structure is schematically illustrated in Fig. 1. A thin film of molybdenum, which serves as a seed layer for the growth of $MoS_2$, was deposited by e-beam evaporation [21]. The Mo-deposited substrate was loaded into the PECVD chamber for sulfurization. Sulfurization at 300 °C under $H_2S$ and Ar plasma atmosphere for 1.5 h led to the formation of MGH.

### 2.3. Characterization

The crystallinity and number of layers of graphene and MGH were characterized by Raman spectroscopy (Alpha300 M+, WITec GmbH,

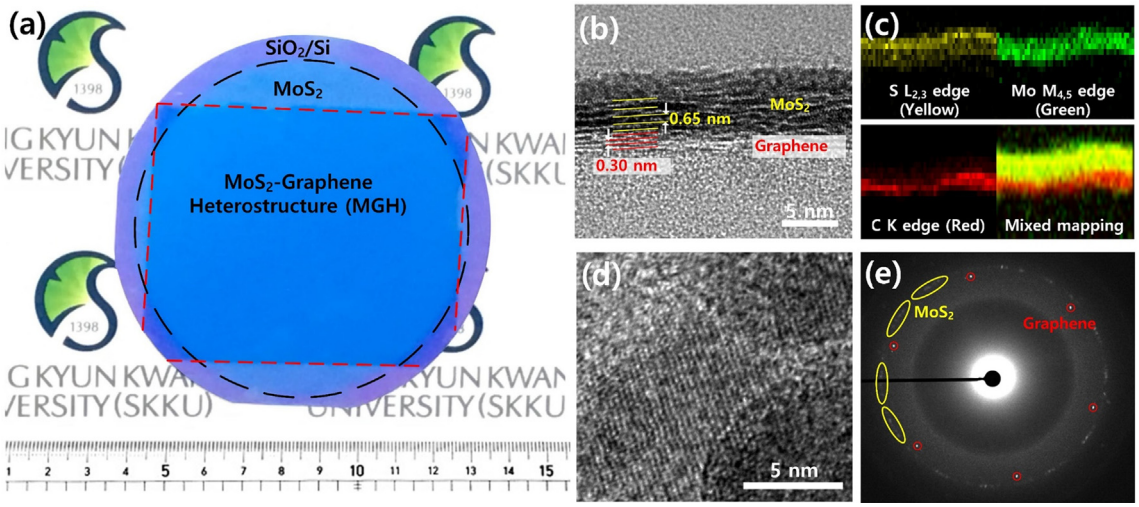


**Fig. 2.** (a) A photograph of wafer-scale MGH on a 4-inch $SiO_2$/Si substrate. The rectangular (red dashed) and the circular (black dashed) regions indicate MGH and bare $MoS_2$ on $SiO_2$/Si substrate, respectively. (b) Cross-sectional HR-TEM images of MGH (c) Electron energy loss spectroscopy elemental mapping images of MGH, which are derived from the Mo $M_{4,5}$, S $L_{2,3}$, and C *K* ionization edges. (d) In-plane HR-TEM image of MGH (e) SAED pattern of the MGH shown in Fig. 2(d).

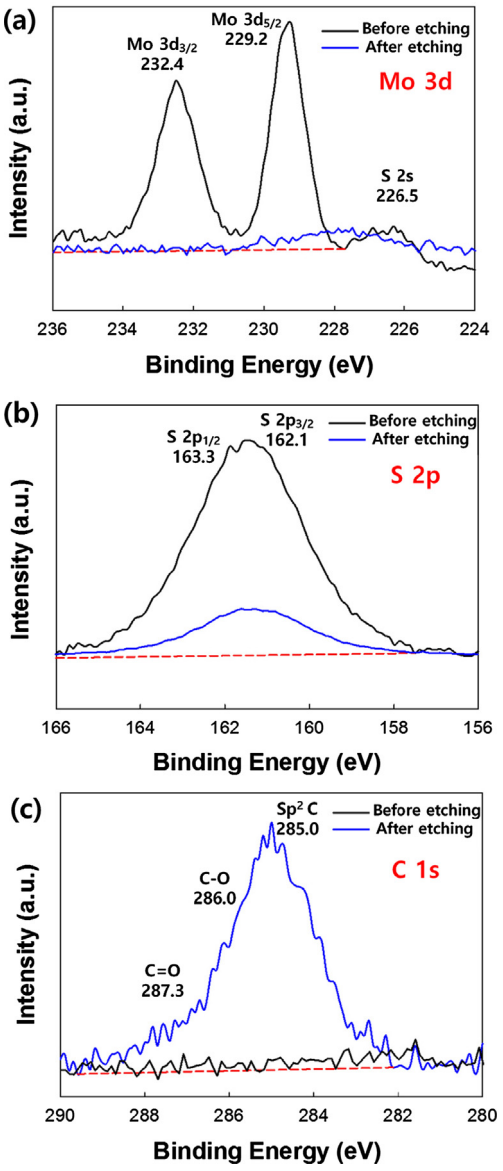


**Fig. 3.** XPS spectra of an MGH thin film before and after Ar etching for depth profiling (a) Mo 3d (b) S 2p for $MoS_2$ and (c) C 1s for graphene, respectively.

excitation wavelength of 532 nm and laser power of 2 mW) and HR-TEM (JEM-2100F, JEOL). Samples for cross sectional transmission electron microscopy (TEM) imaging were fabricated using a focused ion beam (FIB, NX2000, HITACHI Ltd.) with a lift-out technique. The TEM samples were etched using $Ga^+$ ion beam from 30 keV to 5 keV during the FIB milling process. Then a low-energy $Ar^+$ ion beam of 1 keV was used for final milling to minimize surface damage. The respective chemical compositions of the samples were determined by X-ray photoelectron spectroscopy (XPS, MultiLab 2000, Thermo VG) with Mg Kα X-ray source; during XPS, the take-off angle of the MGH was maintained at 45°. Topological profiles of the thin layers were measured using atomic force microscopy (AFM, NX-100, Park system) and electrochemical data were recorded using an Autolab PGSTAT302N potentiostat (Metrohm Autolab B.V.).

### 2.4. Electrochemical measurements

All the electrochemical measurements were carried out with a standard three electrode cell using a potentiostat (Autolab PGSTAT302N). A graphite rod (Sigma-Aldrich, 99.995%) and a saturated calomel electrode (saturated KCl) were used as the counter and reference electrodes (SCE, 0.256 V vs. RHE in 0.5 M $H_2SO_4$), respectively; all the measured potentials were referenced to the reversible hydrogen electrode (RHE) potential. Linear sweep voltammograms (LSV) were traced using a glassy carbon electrode (GCE) (0.196 $cm^2$, Pine Research Instrumentation, USA) at a scan rate of 2 mV $s^{-1}$ and rotation speed of 1600 rpm. Electrochemical impedance spectroscopy (EIS) was performed in the frequency range 0.01–100,000 Hz at −0.4 V (versus RHE) to determine the series resistance ($R_s$) and charge-transfer resistance ($R_{ct}$). All the data presented were corrected with $R_s$. The GCE was polished with a 0.05 μm $Al_2O_3$ (Buehler) slurry, rinsed with deionized (DI) water, cleaned in water for 10 s using an ultrasonic cleaner and then washed once again with DI water. The bare glassy carbon electrode was polished to a mirror surface using 0.3 and 0.05 μm $Al_2O_3$ powders, consecutively, and thoroughly rinsed twice with DI water between each polishing step. Next, the electrode was washed successively in ultra-sonic bath with 1:1 (v/v) $HNO_3$ aqueous solution, twice in DI water, once in ethanol, and again twice in DI water; finally, the clean electrode was dried in air.

## 3. Results and discussion

A photograph of the 100-$cm^2$-area MGH (dark blue rectangular region) shows highly uniform growth of MGH on the 4-inch $SiO_2$/Si wafer in Fig. 2(a). HR-TEM was conducted to determine both the number of layers and the crystallinity of the MGH. Cross sectional HR-TEM image of MGH and its corresponding electron energy loss spectroscopy elemental mapping images show that top $MoS_2$ layers of total thickness 6–7 nm are uniformly and continuously grown on the underlying graphene (Fig. 2(b) and (c)). The *d*-spacing of the $MoS_2$ layers (yellow line) and graphene (red line) is 0.63–0.65 nm and 0.30–0.32 nm, respectively, which is consistent with that measured for typical bulk $MoS_2$ and graphite (Fig. 2(b)) [15]. An in-plane HR-TEM image of MGH in Fig. 2(d) depicts the overlapping of $MoS_2$ and graphene layers with grain boundaries. The corresponding selected area electron diffraction (SAED) patterns of the MGH consist of single (red circles) and multiple (yellow circles) sets of diffractions spots with six-fold symmetry originating from the top layer of the nanocrystalline $MoS_2$ and the bottom graphene layer, respectively, as depicted in Fig. 2(e). We also confirmed that the crystallinity of the bare $MoS_2$ is similar to that of the MGH in Fig. S1. The overall crystal structure of MGH was elucidated by XRD, where four diffraction peaks at 2θ values of 14.5°, 33°, 39°, and 59°, corresponding to the (0 0 2), (1 0 0), (1 0 3), and (1 1 0) planes, respectively, are seen, as marked in Fig. S2 (JCPDS 37-1492). We note here that the strong (0 0 2) reflection confirms the presence of the layered structure of $MoS_2$ [34]. The topology of the MGH was investigated by AFM and the root mean square (RMS) value is estimated to be 1.95 nm (Fig. S3).

The chemical states of both the top-$MoS_2$ film and the bottom-graphene layer in the MGH were analyzed sequentially by depth profiling XPS [35]. The Mo(3d) and S(2p) XPS spectra are presented in Fig. 3(a) and (b). The binding energies of the $Mo^{4+}$ 3d peaks at 229.2 and 232.4 eV corresponding to Mo $3d_{5/2}$ and Mo $3d_{3/2}$, respectively, and the $S^{2-}$ 2p peaks at 162.1 and 163.3 eV, corresponding to the S $2p_{3/2}$ and S $2p_{1/2}$, respectively, confirm the elemental composition of $MoS_2$ on the surface of the MGH. The atomic ratio of S to Mo is found to be 1.78, which is close to the stoichiometric value of 2 in $MoS_2$ (Fig. S4) [36]. After measuring the XPS of the $MoS_2$ layer, plasma etching was carried out by $Ar^+$ ion beam (4 kW, 6 μA, 3 min). It is seen that after plasma etching, the signals originating from $MoS_2$ layers disappear but those from the underlying graphene appear. The binding energies of 284.6 eV, 285.2 eV, and 287.1 eV in the C1s core level spectral region, due to $sp^2$ carbon-carbon, $sp^3$ carbon-carbon, and carbon-oxygen bonds, respectively, indicate that the carbon atoms maintained the honeycomb structure and are not chemically bonded to Mo and S [37].

To explore the effects of graphene during sulfurization, we have

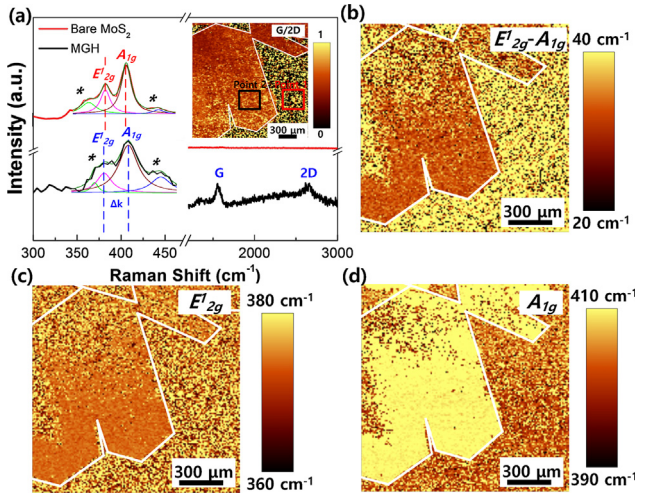


**Fig. 4.** (a) Representative Raman spectra of MGH and bare $MoS_2$ at the marked regions (inset shows the Raman mapping of the integrated intensity ratio of the G and 2D). Raman mapping image of MGH for (b) $E^1_{2g} - A_{1g}$, (c) $E^1_{2g}$ and (d) $A_{1g}$ peak, respectively.

simultaneously grown $MoS_2$ on both graphene and amorphous $SiO_2$ surfaces; more details on the preparation of partially grown graphene and its transfer on $SiO_2$/Si substrate are described in Fig. S5. The Raman spectra from both the MGH (black line) and bare $MoS_2$ (red line) show strong and broad peaks at 373–379 $cm^{-1}$ and 400–406 $cm^{-1}$, which correspond to the in-plane vibration mode ($E^1_{2g}$) and out-of-plane vibration mode ($A_{1g}$), respectively, with weak defect-related satellite Raman peaks (marked as * in Fig. 4 (a)) [38]. In comparison to bare $MoS_2$, the $A_{1g}$ peak for the MGH is upshifted and the peak separation between $E^1_{2g}$ and $A_{1g}$ (Δk) is increased, indicating that the density of defects increases during sulfurization on the graphene (Fig. 4(b–d)) [13,39]. Interestingly, intensity of peak at 448 $cm^{-1}$, which correspond to the S vacancy in $MoS_2$, is significantly increased [38]. Thus, we may infer that the density of point defects (e.g. sulfur vacancies) in MGH should be higher than that in bare $MoS_2$ [40]. The lattice constant difference of typical metal and $MoS_2$ is less than 1%, while that of graphene and $MoS_2$ is about 21.9%. Therefore, growing $MoS_2$ on the graphene, which has the hexagonal crystal structure and strong interaction, may induce large numbers of point defects compared to growing $MoS_2$ on the amorphous $SiO_2$ surface [41–43]. We also note that the S/Mo stoichiometry of MGH from XPS is slightly decrease to 1.78, which indicates a reduction in the total amount of sulfur (Fig. S4). Compared to the Raman spectrum of pristine graphene on $SiO_2$/Si substrate, the intensities of the G peak (~1580 $cm^{-1}$), and 2D peak (~2580 $cm^{-1}$) are not significantly changed after $MoS_2$ growth, suggesting that the hexagonal carbon structure of graphene is not notably affected by plasma during sulfurization [44].

To exploit the properties of crystalline $MoS_2$ on conducting graphene, we have investigated the MGH as a catalyst for hydrodesulfurization and as an electro-catalyst in the HER [45]. To demonstrate its catalytic activity, we transferred the MGH film onto a mirror-polished GCE as shown in Fig. S6. Due to the very weak interaction between the graphene layer and the $SiO_2$ surface, it was possible to delaminate the MGH even in the presence of a $MoS_2$ film on graphene [2,46]. For comparison, we transferred a bare $MoS_2$ film on to the pristine GCE using a conventional transfer process. (See Fig. S7)

Electrochemical measurements were performed in 0.5 M $H_2SO_4$ solution using a typical three-electrode cell setup; the cathodic polarization curves and Tafel plots are shown in Fig. 5. It is seen that 20% Pt/C exhibits a near-zero potential and has the highest HER activity when compared to other catalysts [47,48]. In contrast, the GCE and pristine graphene on GCE electrodes do not show any catalytic behavior.

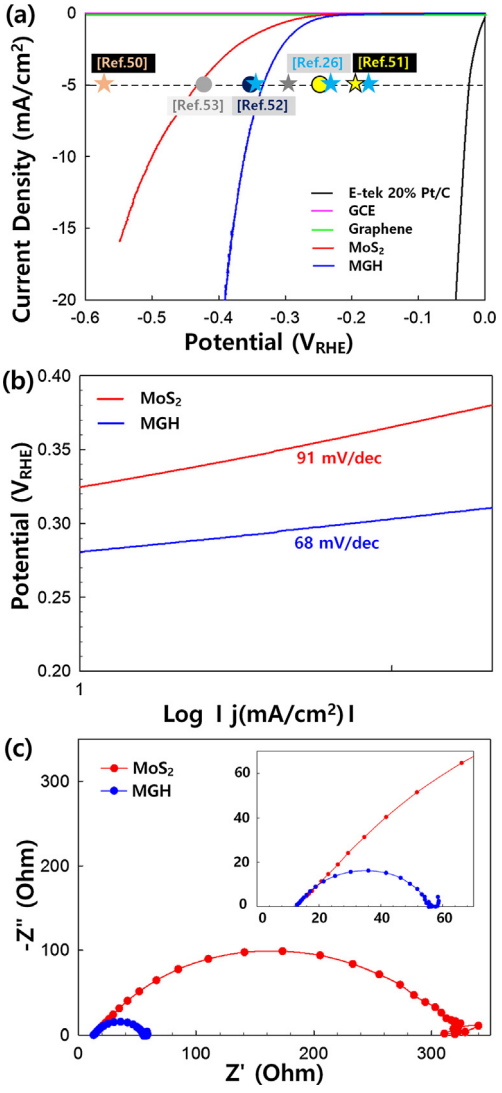


**Fig. 5.** Electrochemical HER performances of MGH and bare $MoS_2$ on GEC. (a) Polarization curves measured by LSV along with results from previously published works (b) Tafel plots obtained from polarization curves. (c) EIS of MGH and bare $MoS_2$ fabricated at 300 °C on GCE; inset shows the spectrum for the specific range from 0 to 70 Ω.

However, the onset over-potential (η) and Tafel slope of the MGH were 0.21 V and 68 mV/dec, which was lower than that of bare $MoS_2$, pointing to the enhanced catalytic performance of the MGH [49]. It is noted here that MGH shows a better catalytic activity than those previously reported for CVD grown $MoS_2$ (including exfoliated $MoS_2$) as shown in Table 1. The onset η values are labeled by stars or circles of different colors in Fig. 5(a) [26,50–53]. The star indicates some sort of treatment such as plasma, annealing, chemical exfoliation, and vacancy for the sample, whereas, those marked by circles indicate that the sample was not subjected to any treatment; the details of the different procedures are given in Table 1. EIS was used to further study the interfacial reactions and electrode kinetics during HER processes for MGH and the bare $MoS_2$ electrodes. Although the difference in ohmic resistance between the two films is negligible, the charge-transfer resistance of 42 O (Ω) for the MGH film is significantly lower than that of bare $MoS_2$, which is 311 Ω as shown in Fig. 5(c) [51,54]. Thus, the enhanced catalytic activity of the MGH film electrode can be attributed to be due the following: (1) The large density of grain boundaries and sulfur vacancies on the basal plane in the MGH structure, which give rise to a high density of active sites. (2) The efficient charge transport

**Table 1**
. A comparison between the various $MoS_2$-derived HER catalysts in acidic electrolytes.

| Catalyst | Synthetic method | Temperature (°C) | η at 5 mA $cm^{-2}$ (V) | Tafel slope (mV $dec^{-1}$) | Refs. |
|---|---|---|---|---|---|
| $MoS_2$ | PECVD | 300 | 0.43 | 91 | Present work |
| MGH | | | 0.33 | 68 | |
| $MoS_2$/Au | Mo is evaporated in $H_2S$ atmosphere | 550 | – | 50–60 | [45] |
| $O_2$ plasma- treated $MoS_2$ | Oxygen plasma treatment after CVD growth | 750 | 0.56 | 171 | [50] |
| $H_2$-annealed $MoS_2$ (500 °C) | Hydrogen annealing after CVD growth | | 0.56 | 147 | |
| 2H $MoS_2$ | 1 T $MoS_2$ converts to 2H $MoS_2$ | 300 | 0.26 | 75–85 | [51] |
| 1 T $MoS_2$ | Chemical exfoliation | 300 | 0.19 | 40 | |
| Strained vacancy $MoS_2$ | CVD | 750 | 0.17 | 60 | [26] |
| Vacancy $MoS_2$ | | | 0.22 | 82 | |
| Edge-terminated $MoS_2$ | | | 0.36 | 90 | |
| Edge- terminated $MoS_2$ | CVD | 550 | 0.37 | 86 | [52] |
| 1 T $MoS_2$ | Hydrolysis exfoliation | 1000 | 0.30 | 98 | [53] |
| 2H $MoS_2$ | | 400 | 0.45 | 150 | |

pathway through the highly conductive graphene layer from the active sites in $MoS_2$ to the electrode in the MGH film [29,31]. (3) The reduction of band gap at the domain edge of nanocrystalline MGH, which sufficiently decrease hydrogen recombination barrier [55].

## 4. Conclusion

In conclusion, we have successfully synthesized a 4 inch sized $MoS_2$-on-graphene heterostructure through a $H_2S$ sulfurization process. The Raman and HR-TEM results reveal that 5–6 $MoS_2$ layers with a large density of sulfur vacancies and grain boundaries are uniformly grown on the entire substrate. To exploit the nanocrystalline MGH film containing a high sulfur vacancy concentration, we investigated the MGH as a catalyst for hydro-desulfurization and as an electro-catalyst for the HER. When compared to $MoS_2$ grown from an amorphous $SiO_2$ substrate, the MGH electrodes have smaller onset potential and Tafel slope, indicating their enhanced catalytic performance. This enhancement can be attributed to the high density of defects (grain boundaries and sulfur vacancies) present in $MoS_2$ synthesized on graphene, which while increasing the total number of active sites, provide an effective charge transport pathway through the highly conducting graphene layer. We believe that this study will lead to the development of practical strategies for the large-scale synthesis of various 2D heterostructures at low temperatures and thus promote their use in a wide range of applications.

## Acknowledgment

This work was supported by the Presidential Postdoctoral Fellowship Program of the Ministry of Education, through the NRF (2014R1A6A3A04058169) and NRF-2017R1A2B3011222. This research was supported by Basic Science Research Program through the National Research Foundation of Korea (NRF) funded by the Ministry of Education (2018R1D1A1B07040292).

## Appendix A. Supplementary material

Supplementary data to this article can be found online at https://doi.org/10.1016/j.apsusc.2018.11.126.

## References

[1] K. Roy, M. Padmanabhan, S. Goswami, T.P. Sai, G. Ramalingam, S. Raghavan, A. Ghosh, Graphene–$MoS_2$ hybrid structures for multifunctional photoresponsive memory devices, Nat. Nanotechnol. 8 (2013) 826.
[2] A.K. Geim, Graphene: status and prospects, Science 324 (2009) 1530–1534.
[3] Y.H. Lee, X.Q. Zhang, W. Zhang, M.T. Chang, C.T. Lin, K.D. Chang, Y.C. Yu, J.T.W. Wang, C.S. Chang, L.J. Li, Synthesis of large-area $MoS_2$ atomic layers with chemical vapor deposition, Adv. Mater. 24 (2012) 2320–2325.
[4] Y. Zhang, Y. Zhang, Q. Ji, J. Ju, H. Yuan, J. Shi, T. Gao, D. Ma, M. Liu, Y. Chen, Controlled growth of high-quality monolayer $WS_2$ layers on sapphire and imaging its grain boundary, ACS Nano 7 (2013) 8963–8971.
[5] A. Gurarslan, Y. Yu, L. Su, Y. Yu, F. Suarez, S. Yao, Y. Zhu, M. Ozturk, Y. Zhang, L. Cao, Surface-energy-assisted perfect transfer of centimeter-scale monolayer and few-layer $MoS_2$ films onto arbitrary substrates, ACS Nano 8 (2014) 11522–11528.
[6] H. Van Ngoc, Y. Qian, S.K. Han, D.J. Kang, PMMA-etching-free transfer of wafer-scale chemical vapor deposition two-dimensional atomic crystal by a water soluble polyvinyl alcohol polymer method, Sci. Rep. 6 (2016) 33096.
[7] Y. Fang, Y. Lv, F. Gong, A.A. Elzatahry, G. Zheng, D. Zhao, Synthesis of 2D-mesoporous-carbon/$MoS_2$ heterostructures with well-defined interfaces for high-performance lithium-ion batteries, Adv. Mater. 28 (2016) 9385–9390.
[8] L. Ma, X. Zhou, L. Xu, X. Xu, L. Zhang, W. Chen, Chitosan-assisted fabrication of ultrathin $MoS_2$/graphene heterostructures for Li-ion battery with excellent electrochemical performance, Electrochim. Acta 167 (2015) 39–47.
[9] J. Liang, J. Li, H. Zhu, Y. Han, Y. Wang, C. Wang, Z. Jin, G. Zhang, J. Liu, One-step fabrication of large-area ultrathin $MoS_2$ nanofilms with high catalytic activity for photovoltaic devices, Nanoscale 8 (2016) 16017–16025.
[10] M.F. Khan, M.A. Shehzad, M.Z. Iqbal, M.W. Iqbal, G. Nazir, Y. Seo, J. Eom, A facile route to a high-quality graphene/$MoS_2$ vertical field-effect transistor with gate-modulated photocurrent response, J. Mater. Chem. C 5 (2017) 2337–2343.
[11] Y. Lee, J. Lee, H. Bark, I.-K. Oh, G.H. Ryu, Z. Lee, H. Kim, J.H. Cho, J.-H. Ahn, C. Lee, Synthesis of wafer-scale uniform molybdenum disulfide films with control over the layer number using a gas phase sulfur precursor, Nanoscale 6 (2014) 2821–2826.
[12] Y. Shi, W. Zhou, A.-Y. Lu, W. Fang, Y.-H. Lee, A.L. Hsu, S.M. Kim, K.K. Kim, H.Y. Yang, L.-J. Li, van der Waals epitaxy of $MoS_2$ layers using graphene as growth templates, Nano Lett. 12 (2012) 2784–2791.
[13] J.A. Miwa, M. Dendzik, S.S. Grønborg, M. Bianchi, J.V. Lauritsen, P. Hofmann, S. Ulstrup, van der Waals epitaxy of two-dimensional $MoS_2$–graphene heterostructures in ultrahigh vacuum, ACS Nano 9 (2015) 6502–6510.
[14] H. Ago, H. Endo, P. Solís-Fernández, R. Takizawa, Y. Ohta, Y. Fujita, K. Yamamoto, M. Tsuji, Controlled van der Waals epitaxy of monolayer $MoS_2$ triangular domains on graphene, ACS Appl. Mater. Interface 7 (2015) 5265–5273.
[15] J. Jeon, S.K. Jang, S.M. Jeon, G. Yoo, Y.H. Jang, J.-H. Park, S. Lee, Layer-controlled CVD growth of large-area two-dimensional $MoS_2$ films, Nanoscale 7 (2015) 1688–1695.
[16] Y. Zhan, Z. Liu, S. Najmaei, P.M. Ajayan, J. Lou, Large-area vapor-phase growth and characterization of $MoS_2$ atomic layers on a $SiO_2$ substrate, Small 8 (2012) 966–971.
[17] X. Wang, H. Feng, Y. Wu, L. Jiao, Controlled synthesis of highly crystalline $MoS_2$ flakes by chemical vapor deposition, JACS 135 (2013) 5304–5307.
[18] J. Mun, Y. Kim, I.-S. Kang, S.K. Lim, S.J. Lee, J.W. Kim, H.M. Park, T. Kim, S.-W. Kang, Low-temperature growth of layered molybdenum disulphide with controlled clusters, Sci. Rep. 6 (2016) 21854.
[19] H. Takeuchi, A. Wung, X. Sun, R.T. Howe, T.-J. King, Thermal budget limits of quarter-micrometer foundry CMOS for post-processing MEMS devices, IEEE Trans. Elect. Dev. 52 (2005) 2081–2086.
[20] V.T. Renard, M. Jublot, P. Gergaud, P. Cherns, D. Rouchon, A. Chabli, V. Jousseaume, Catalyst preparation for CMOS-compatible silicon nanowire synthesis, Nat. Nanotechnol. 4 (2009) 654.
[21] C. Ahn, J. Lee, H.U. Kim, H. Bark, M. Jeon, G.H. Ryu, Z. Lee, G.Y. Yeom, K. Kim, J. Jung, Low-temperature synthesis of large-scale molybdenum disulfide thin films directly on a plastic substrate using plasma-enhanced chemical vapor deposition, Adv. Mater. 27 (2015) 5223–5229.
[22] S. Kataria, S. Wagner, J. Ruhkopf, A. Gahoi, H. Pandey, R. Bornemann, S. Vaziri, A.D. Smith, M. Ostling, M.C. Lemme, Chemical vapor deposited graphene: From synthesis to applications, Phys. Status Solidi A 211 (2014) 2439–2449.
[23] H. Kim, C. Ahn, G. Arabale, C. Lee, T. Kim, Synthesis of $MoS_2$ atomic layer using PECVD, ECS Trans. 58 (2013) 47–50.

[24] H.-U. Kim, H. Kim, C. Ahn, A. Kulkarni, M. Jeon, G.Y. Yeom, M.-H. Lee, T. Kim, In situ synthesis of $MoS_2$ on a polymer based gold electrode platform and its application in electrochemical biosensing, RSC Adv. 5 (2015) 10134–10138.
[25] S. Kim, A. Konar, W. Hwang, J. Lee, J. Lee, J. Yang, C. Jung, H. Kim, J. Yoo, J.Y. Choi, Y.W. Jin, S.Y. Lee, D. Jena, W. Choi, K. Kim, Nat. Commun 3 (2012) 1011.
[26] H. Li, C. Tsai, A.L. Koh, L. Cai, A.W. Contryman, A.H. Fragapane, J. Zhao, H.S. Han, H.C. Manoharan, F. Abild-Pedersen, Activating and optimizing $MoS_2$ basal planes for hydrogen evolution through the formation of strained sulphur vacancies, Nat. Mater. 15 (2016) 48.
[27] J. Liang, C. Wang, P. Zhao, Y. Wang, L. Ma, G. Zhu, Y. Hu, Z. Lu, Z. Xu, Y. Ma, Interface engineering of anchored ultrathin $TiO_2$/$MoS_2$ heterolayers for highly-efficient electrochemical hydrogen production, ACS Appl. Mater. Interface 10 (2018) 6084–6089.
[28] X. Xu, Y. Sun, W. Qiao, X. Zhang, X. Chen, X. Song, L. Wu, W. Zhong, Y. Du, 3D $MoS_2$-graphene hybrid aerogels as catalyst for enhanced efficient hydrogen evolution, Appl. Surf. Sci. 396 (2017) 1520–1527.
[29] M. Wen, T. Xiong, Z. Zang, W. Wei, X. Tang, F. Dong, Synthesis of $MoS_2$/$gC_3N_4$ nanocomposites with enhanced visible-light photocatalytic activity for the removal of nitric oxide (NO), Opt. Exp. 24 (2016) 10205–10212.
[30] J. Liang, G. Zhu, C. Wang, Y. Wang, H. Zhu, Y. Hu, H. Lv, R. Chen, L. Ma, T. Chen, $MoS_2$-based all-purpose fibrous electrode and self-powering energy fiber for efficient energy harvesting and storage, Adv. Energy Mater. 7 (2017) 1601208.
[31] Y. Li, H. Wang, L. Xie, Y. Liang, G. Hong, H. Dai, $MoS_2$ nanoparticles grown on graphene: an advanced catalyst for the hydrogen evolution reaction, JACS 133 (2011) 7296–7299.
[32] L. Ma, Y. Hu, G. Zhu, R. Chen, T. Chen, H. Lu, Y. Wang, J. Liang, H. Liu, C. Yan, In situ thermal synthesis of inlaid ultrathin $MoS_2$/graphene nanosheets as electrocatalysts for the hydrogen evolution reaction, Chem. Mater. 28 (2016) 5733–5742.
[33] B. Hinnemann, P.G. Moses, J. Bonde, K.P. Jørgensen, J.H. Nielsen, S. Horch, I. Chorkendorff, J.K. Nørskov, Biomimetic hydrogen evolution: $MoS_2$ nanoparticles as catalyst for hydrogen evolution, JACS 127 (2005) 5308–5309.
[34] D.H. Youn, J.-W. Jang, J.Y. Kim, J.S. Jang, S.H. Choi, J.S. Lee, Fabrication of graphene-based electrode in less than a minute through hybrid microwave annealing, Sci. Rep. 4 (2014) 5492.
[35] J.B. Gilbert, M.F. Rubner, R.E. Cohen, Depth-profiling X-ray photoelectron spectroscopy (XPS) analysis of interlayer diffusion in polyelectrolyte multilayers, Proc. Natl. Acad. Sci. 110 (2013) 6651–6656.
[36] P. Beccat, P. Da Silva, Y. Huiban, S. Kasztelan, Quantitative surface analysis by XPS (X-ray photoelectron spectroscopy): application to hydrotreating catalysts, Oil Gas Sci. Technol. 54 (1999) 487–496.
[37] K. Emtsev, F. Speck, T. Seyller, L. Ley, J.D. Riley, Interaction, growth, and ordering of epitaxial graphene on SiC 0001 surfaces: a comparative photoelectron spectroscopy study, Phys. Rev. B 77 (2008) 155303.
[38] S. Bae, N. Sugiyama, T. Matsuo, H. Raebiger, K.-I. Shudo, K. Ohno, Defect-induced vibration modes of Ar + -irradiated $MoS_2$, Phys. Rev. Appl 7 (2017) 024001.
[39] W.M. Parkin, A. Balan, L. Liang, P.M. Das, M. Lamparski, C.H. Naylor, J.A. Rodríguez-Manzo, A.C. Johnson, V. Meunier, M. Drndić, Raman shifts in electron-irradiated monolayer $MoS_2$, ACS Nano 10 (2016) 4134–4142.
[40] Y. Ma, Y. Dai, M. Guo, C. Niu, B. Huang, Graphene adhesion on $MoS_2$ monolayer: an ab initio study, Nanoscale 3 (2011) 3883–3887.
[41] M. Farmanbar, G. Brocks, First-principles study of van der Waals interactions and lattice mismatch at $MoS_2$/metal interfaces, Phys. Rev. B 93 (2016) 085304.
[42] M. Liu, J. Shi, Y. Li, X. Zhou, D. Ma, Y. Qi, Y. Zhang, Z. Liu, Temperature-triggered sulfur vacancy evolution in monolayer $MoS_2$/graphene heterostructures, Small 13 (2017) 1602967.
[43] J. Shi, M. Liu, J. Wen, X. Ren, X. Zhou, Q. Ji, D. Ma, Y. Zhang, C. Jin, H. Chen, All chemical vapor deposition synthesis and intrinsic bandgap observation of $MoS_2$/graphene heterostructures, Adv. Mater. 27 (2015) 7086–7092.
[44] A.C. Ferrari, J. Meyer, V. Scardaci, C. Casiraghi, M. Lazzeri, F. Mauri, S. Piscanec, D. Jiang, K. Novoselov, S. Roth, Raman spectrum of graphene and graphene layers, Phys. Rev. Lett. 97 (2006) 187401.
[45] T.F. Jaramillo, K.P. Jørgensen, J. Bonde, J.H. Nielsen, S. Horch, I. Chorkendorff, Identification of active edge sites for electrochemical $H_2$ evolution from $MoS_2$ nanocatalysts, Sci 317 (2007) 100–102.
[46] J.-H. Lee, E.K. Lee, W.-J. Joo, Y. Jang, B.-S. Kim, J.Y. Lim, S.-H. Choi, S.J. Ahn, J.R. Ahn, M.-H. Park, Wafer-scale growth of single-crystal monolayer graphene on reusable hydrogen-terminated germanium, Science 344 (2014) 286–289.
[47] J. Greeley, T.F. Jaramillo, J. Bonde, I. Chorkendorff, J.K. Nørskov, Computational high-throughput screening of electrocatalytic materials for hydrogen evolution, Nat. Mater. 5 (2006) 909.
[48] J. Greeley, I. Stephens, A. Bondarenko, T.P. Johansson, H.A. Hansen, T. Jaramillo, J. Rossmeisl, I. Chorkendorff, J.K. Nørskov, Alloys of platinum and early transition metals as oxygen reduction electrocatalysts, Nat. Chem. 1 (2009) 552.
[49] W. Fu, F.-H. Du, J. Su, X.-H. Li, X. Wei, T.-N. Ye, K.-X. Wang, J.-S. Chen, In situ catalytic growth of large-area multilayered graphene/$MoS_2$ heterostructures, Sci. Rep. 4 (2014) 4673.
[50] G. Ye, Y. Gong, J. Lin, B. Li, Y. He, S.T. Pantelides, W. Zhou, R. Vajtai, P.M. Ajayan, Defects engineered monolayer $MoS_2$ for improved hydrogen evolution reaction, Nano Lett. 16 (2016) 1097–1103.
[51] D. Voiry, M. Salehi, R. Silva, T. Fujita, M. Chen, T. Asefa, V.B. Shenoy, G. Eda, M. Chhowalla, Conducting $MoS_2$ nanosheets as catalysts for hydrogen evolution reaction, Nano Lett. 13 (2013) 6222–6227.
[52] D. Kong, H. Wang, J.J. Cha, M. Pasta, K.J. Koski, J. Yao, Y. Cui, Synthesis of $MoS_2$ and $MoSe_2$ films with vertically aligned layers, Nano Lett. 13 (2013) 1341–1347.
[53] K. Chang, X. Hai, H. Pang, H. Zhang, L. Shi, G. Liu, H. Liu, G. Zhao, M. Li, J. Ye, Targeted synthesis of 2H-and 1T-phase $MoS_2$ monolayers for catalytic hydrogen evolution, Adv. Mater. 28 (2016) 10033–10041.
[54] C. Shih, C.-J. Shih, Q.H. Wang, Y. Son, Z. Jin, D. Blankschtein, M.S. Strano, ACS Nano 8 (2014) 5790.
[55] J. Shi, X. Zhou, G.F. Han, M. Liu, D. Ma, J. Sun, C. Li, Q. Ji, Y. Zhang, X. Song, Narrow-gap quantum wires arising from the edges of monolayer $MoS_2$ synthesized on graphene, Adv. Mater. Interface 3 (2016) 1600332.